# Enhancement of the Strength and the Corrosion Resistance of a PT-7M Titanium Alloy Using Rotary Forging

**V. N. Chuvil'deev**[a], **V. I. Kopylov**[a, b], **A. V. Nokhrin**[a, *], **A. M. Bakhmet'ev**[c], **P. V. Tryaev**[c],
**N. Yu. Tabachkova**[d], **M. K. Chegurov**[a], **N. A. Kozlova**[a], **A. S. Mikhailov**[c], **A. V. Ershova**[c],
**M. Yu. Gryaznov**[a], **Ya. S. Shadrina**[a], **K. V. Likhnitskii**[a], **S. P. Stepanov**[a], and **M. M. Myshlyaev**[e]

[a] Lobachevskii National Research State University of Nizhny Novgorod, Nizhny Novgorod, Russia
[b] Physicotechnical Institute, Belarussian Academy of Sciences, Minsk, Belarus
[c] AO Afrikantov Experimental Design Office of Mechanical Engineering, Nizhny Novgorod, Russia
[d] National Research University of Science and Technology MISiS, Moscow, Russia
[e] Baikov Institute of Metallurgy and Materials Science, Russian Academy of Sciences, Moscow, Russia
*e-mail: nokhrin@nifti.unn.ru

**Abstract**—The effect of severe plastic deformation by rotary forging on the mechanical properties and the corrosion resistance of a pseudo-α-titanium PT-7M alloy is studied. The corrosive character of fracture the fine-grained alloy under hot salt corrosion (HSC) conditions is found to change: pitting corrosion at the onset of recrystallization processes changes into intercrystalline corrosion. The HSC resistance of the fine-grained PT-7M titanium alloy is shown to depend on the structure–phase state of grain boundaries, whose intense migration with developing recrystallization leads to "sweeping out" of corrosion-hazardous alloying elements (aluminum, zirconium) from the crystal lattice of the titanium alloy.

## INTRODUCTION

At present, pseudo-α-titanium alloys Ti–(1.8–2.5) wt % Al–(2–3) wt % Zr (industrial PT-7M alloy) are actively used in nuclear engineering and nuclear power engineering for manufacturing heat-exchange equipment of the secondary circuits of a nuclear power plant (NPP).[1] Titanium alloys for MPP must satisfy stringent strength and corrosion resistance requirements [1], which are traditionally attained by optimization of the chemical compositions of the alloys and the heat and/or deformation treatment conditions [2–10].

One of the most hazardous types of fracture of titanium alloy is hot salt corrosion (HSC) [11–14], which is observed at temperatures higher than 200–250°C under conditions of interacting titanium with halide salts (chlorides, bromides, iodides) and in the presence of water (which can exist in a bound state in salt crystalline hydrates, in an occluded state in salt crystals, or in a free state in the air atmosphere). As was shown in [15–17], the structure–phase state of grain boundaries and the formation of a fine-grained (FG) structure during severe plastic deformation (SPD), where the strength and the corrosion resistance increase simultaneously, substantially influence the

---

[1] Hereafter, the compositions are given in wt %.

HSC resistance of pseudo-α-titanium alloys [16, 17]. This approach, in which equal-channel angular pressing is used, provides the refinement of a grain structure and the diffusion redistribution of corrosion-active impurities along grain boundaries of a pseudo-α-titanium alloy [18, 19].

In this work, this approach is used to increase the strength and the corrosion resistance of a PT-7M pseudo-α-titanium alloy, which has a high high-temperature strength and is used for the manufacture of modern NPPs.

## EXPERIMENTAL

In this work, a pseudo-α-titanium PT-7M alloy was used. The alloy chemical composition Ti–2.5% Al–2.6% Zr corresponds to the requirements of State Standard GOST 19807–91. Alloy samples in the initial state were manufactured at AO Chepetsk Mechanical Plant using standard conditions of heat and deformation treatments. An FG structure in the PT-7M alloy was formed using an R5-4-21 HMR rotary forging machine (Germany) by rotary forging (RF) at room temperature [20–22]. From a titanium rod 20 mm in diameter, a rod 6 mm in diameter was fabricated by RF deformation (total cumulative strain is 70%, the strain rate is $0.5–1$ s$^{-1}$). Deformation was

performed by the action of hard-alloy dies on the surface of a titanium rod with its simultaneous rotation.

The structure was studied using a Leica IM DM metallographic microscope, a JEOL JEM-2100 transmission electron microscope equipped with a JED-2300 energy dispersive analyzer, and a JEOL JSM-6490 scanning electron microscope with an INCA 350 energy dispersive microanalyzer. For the studies of a microstructure by metallography and SEM methods, the specimen surfaces were subjected to mechanical grinding and polishing to a roughness of 3−5 μm (diamond paste number was 3/5) with subsequent electrochemical etching in an aqueous 10% HF + 10% $HNO_3$ solution.

X-ray diffraction analysis (XRD) was carried out on a DRON-3 diffractometer. Internal stresses $\sigma_{int}$ were calculated using the Williamson−Hall method and the slope of the curve $(\beta_{hkl})^2 \cos^2 \theta_{hkl} - 16 \sin^2 \theta_{hkl}$ [23], where $\theta_{hkl}$ is the angle corresponding to the intensity maximum of the peak with indices (*hkl*).

The tensile tests of plane 3-mm-thick specimens (specimen no. 23, type I by GOST 1497−84) and cylindrical specimens with a gage part diameter of 3 mm (specimen no. 9, type III according to GOST 1497−84) were carried out at room temperature on a Tinius Olsen H25K-S testing machine. Microhardness $HV_{0.2}$ was measured on an HVS-1000 hardness tester at a load 2 N (0.2 kgf).

Autoclave HSC tests were performed in a mixture of NaCl and KBr salts taken in a proportion of 300 : 1 at a temperature of 250°C using the technique described in [15−17] with access to oxygen. The degree of the corrosion damage was estimated, according to GOST 9.908−85.

Electrochemical studies were carried out using a R-8 potentiostat−galvanostat at room temperature in an aqueous 0.2% HF + 10% $HNO_3$ solution and at a rate of changing the potential (sweep speed) of 0.5 mV/s. Based on an analysis of the Tafel areas of the potentiodynamic potential−current density dependences in semilogarithmic coordinates, we determined corrosion current density $j_{cor}$ and corrosion potential $E_{cor}$. For the studies, 2-mm-thick specimens 15 mm in length and 6 mm in width were cut (the width is equal to the rod diameter after RF). The specimen surfaces were subjected to mechanical grinding and polishing to a roughness of 3−5 μm (diamond paste number 3/5). Finish polishing was carried out by hand to minimize the cold strain of the surface. Before electrochemical tests, the longitudinal section surface of the specimen was covered with a corrosion-resistant protective coating, except for two uncoated (corrosion-active) areas 2 × 5 mm in the central part (zone 1) and in the near-surface part (zone 2) (Fig. 1). Such a specimen structure allowed us to perform comparative studies of the corrosion resistance of the near-surface and central areas of the longitudinal section of FG titanium rods, in which the differences between the microstructure parameters are due to a nonuniform strain distribution from the surface to the center of the
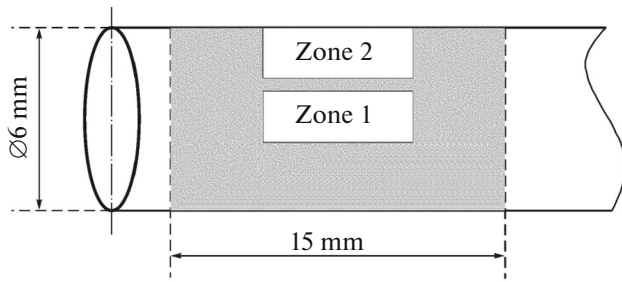


**Fig. 1.** Scheme of cutting a sample (gray) from a titanium rod for corrosion tests and the scheme of analysis sites (zones 1 and 2).

cross section. Before corrosion tests, the specimen surface was subjected to additional electrochemical treatment by the triple (cyclic) measurement of an anode polarization curve at a rate of 5 mV/s.

## RESULTS AND DISCUSSION

In the initial state, the PT-7M alloy has a coarse-grained (CG) lamellar−needle structure (Fig. 2a) with the stitch precipitation of β-phase microparticles along the α'-phase titanium boundary (Fig. 2b), which is typical of α and pseudo-α titanium alloys [1, 24]. The plate thickness of the α' phase of titanium in the initial state of the PT-7M alloy is 5−10 μm, and the length can reach several hundreds of micrometers (Fig. 2a). After RF, a fragmented structure with a mean fragment size ~0.2−0.5 μm forms in the alloy (Figs. 2c, 2d). The reflections in the electron diffraction patterns correspond to α-Ti with a high accuracy. An analysis of the electron diffraction patterns (Fig. 2d) shows that RF leads to the formation of a mainly subgrain structure in the titanium alloy with a low volume fraction of high-angle grain boundaries. The results of the energy dispersive microanalysis show that the boundaries of the fragments of the FG alloy are enriched in zirconium: the local zirconium concentration is 1.6−2.0 wt % in the PT-7M alloy lattice and 3.1−3.6% at the fragment boundaries (Fig. 2e). Note that the increased zirconium concentration at the boundaries of the FG alloy fragments leads to the competing segregation effect: the aluminum concentration in the boundaries of the FG alloy fragments is 1.4−1.8%, which is lower than the aluminum content in grain volume (2.1−2.3%).

Figure 3 shows XRD results for the PT-7M alloy samples in various structural states. The XRD patterns of the coarse- and the fine-grained alloys contain all main peaks corresponding to the α(α') phase.[2] The existence of β-phase particles in the initial and FG alloys were not revealed by XRD, which is likely due to their low volume fraction.

---

[2] Since the crystallographic structures are identical, the XRD peaks of the α and α' phases are indistinguishable in X-ray diffraction patterns.

(a)                   500 μm

(b)                   20 μm

(c)                   0.5 μm

(d)                   5 1/nm

Ti 96.13%
Al 2.12%
Zr 1.75%

⑦

⑧ Ti 94.95%
Al 1.55%
Zr 3.50%

⑨

Ti 96.08%
Al 2.27%
Zr 1.65%

⑩ Ti 95.16%
Al 1.76%
Zr 3.08%

⑪

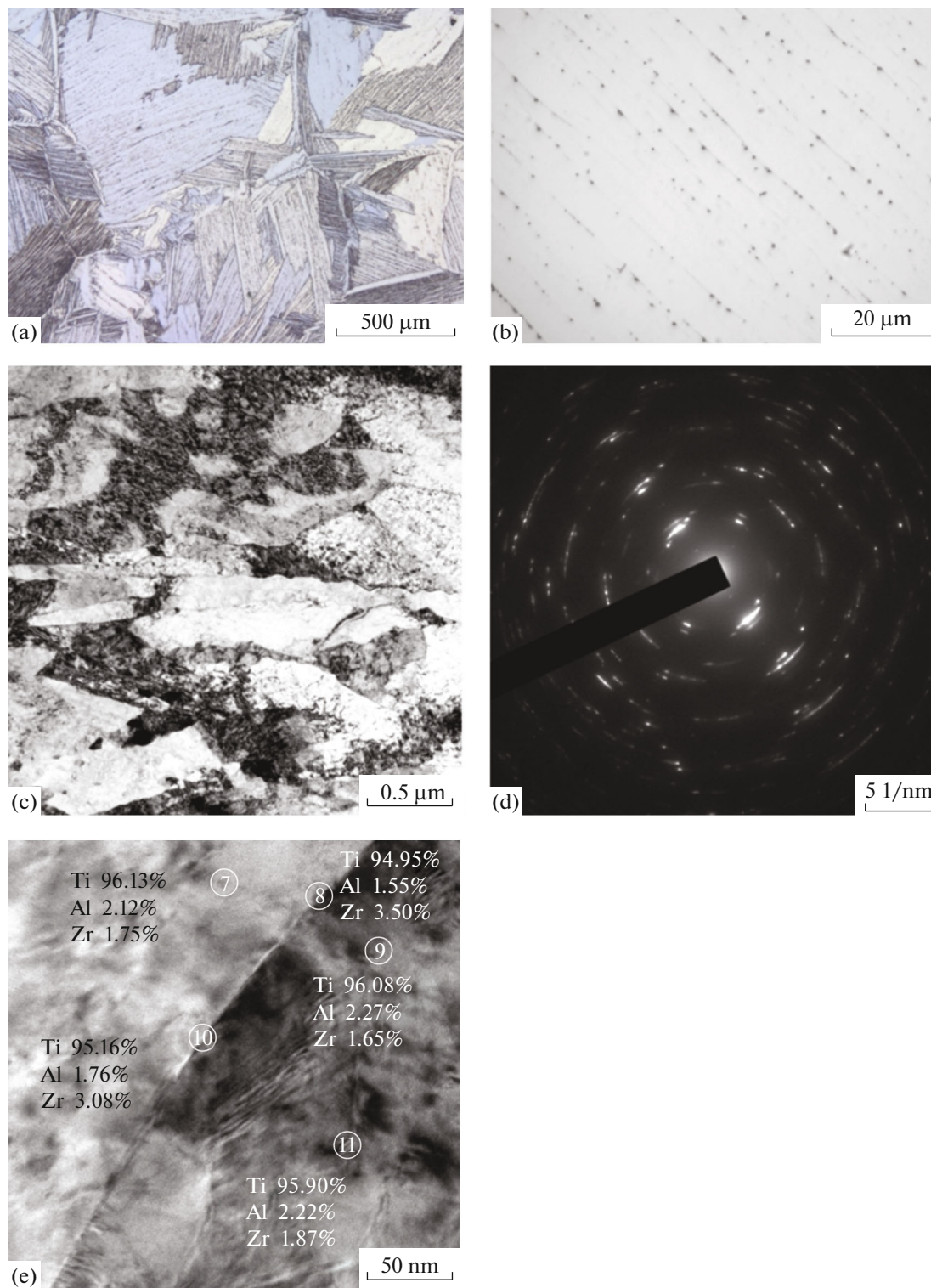Ti 95.90%
Al 2.22%
Zr 1.87%

(e)                   50 nm

**Fig. 2.** Structure of the PT-7M alloy: (a, b) initial state; (c, d) microstructure and electron diffraction pattern of the FG alloy after RF, respectively; (e) results of energy dispersive microanalysis of the grain-boundary composition of the FG PT-7M alloy in the state after RF. (b) Stitch β-phase precipitates along α'-phase grain boundaries.

An analysis of the X-ray diffraction patterns shows that the formation of a FG structure in the PT-7M alloy leads to a broadening of the X-ray peaks of α-Ti with their insignificant shift to the higher reflection angles: diffraction angle $2\theta_{max}$ for the (100) line of α-Ti decreases after RF from 35.11° to 35.05°−35.07°,
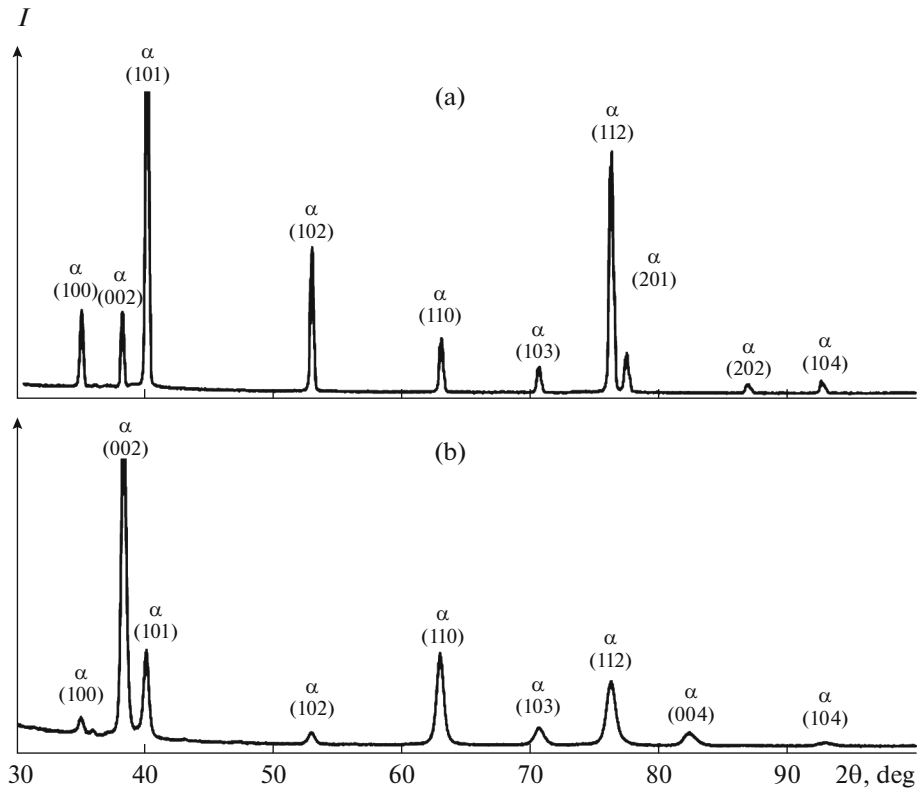
**Fig. 3.** XRD data for the PT-7M alloy: (a) initial state and (b) FG state after RF.

and its half-width at half maximum ($\beta_{0.5}$) increases from 0.308° to 0.554°. The shift of the diffraction maxima to lower diffraction angles according to the Wulff−Bragg equation demonstrates an increase in the $d_{hkl}$ interplanar spacings and the formation of tensile internal stresses $\sigma_{int}$.

The value of $\sigma_{int}$ determined by the Williamson−Hall method is 160 MPa for the initial alloy and 440−520 MPa for the FG alloy. Microhardness $HV_{0.2}$ of the FC alloy sample decreases in the cross section from 2.9−3.0 to 2.5−2.6 GPa in going from the edge to the center of the cross section (hardness in the initial state is ~1.9−2.0 GPa). Mechanical tensile tests showed that the FG structure formation leads to an increase in the yield strength $\sigma_{0.2}$ and ultimate strength $\sigma_u$ of the PT-7M alloy from 280 to 1050−1070 MPa and from 590 to 1080 MPa, respectively. In this case, relative elongation $\delta_5$ decreases from 40 to 6−8%. The stress−strain curves $\sigma(\varepsilon)$ of the coarse-crystal and FG alloys are shown in Fig. 4.

An analysis of the results of the fractographic study after the tensile tests of the PT-7M alloy samples shows that the fracture of the CG alloy sample has a ductile character, which is standard for a titanium α-alloy, with a characteristic slow crack propagation zone and a rupture zone. The area of the fast crack propagation zone in the coarse-crystal alloy is very small as compared to the slow crack propagation zone.

According to the classification of [25], the fracture in the zone of slow (initial) crack propagation consists of equiaxial dimples (Fig. 5a) and the fracture in the rupture zone consists of shear dimples (Fig. 5b).

The fracture surface of the FG PT-7M alloy in the state after RF consists of three zones: the fibrous zone (zone 1 in Fig. 6a, enlarged image in Fig. 6b) corresponding to the slow crack propagation region, the
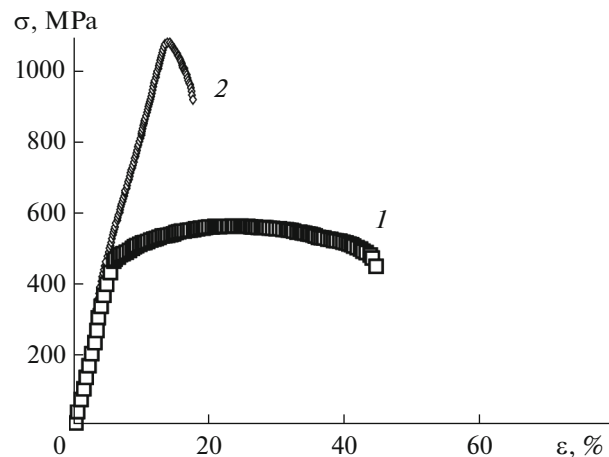


**Fig. 4.** Stress−strain curves for tensile tests of (*1*) CG and (*2*) FG PT-7M alloys.
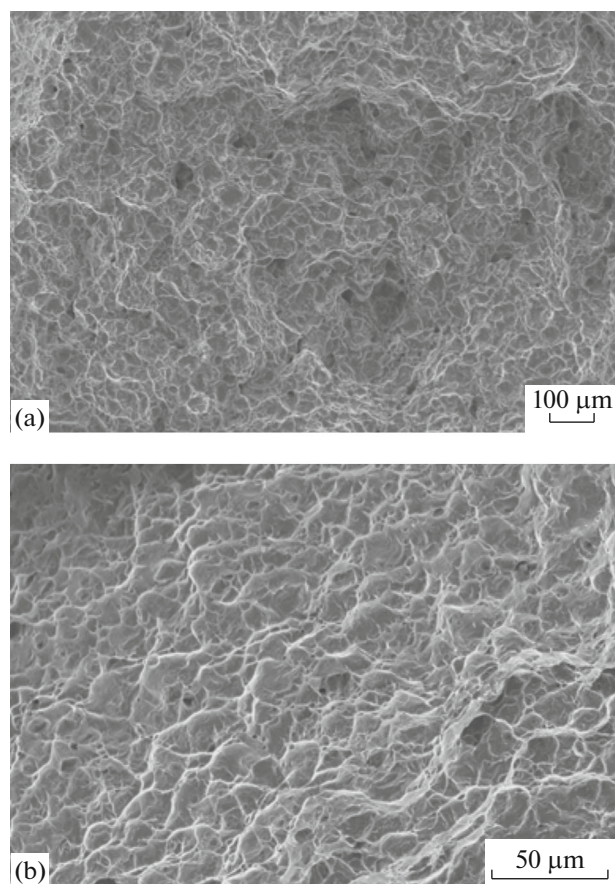
100 μm

(b)
50 μm

**Fig. 5.** SEM micrographs of the fracture surfaces of the CG PT-7M alloy after tensile tests: (a) fibrous zone of slow crack growth and (b) rupture zone.

radial zone (zone 2 in Fig. 6a, enlarged image in Fig. 6c) corresponding to the fast instable crack propagation region, and the rupture zone (zone 3 in Fig. 6a, enlarged image is in Fig. 6d).

It is interesting that the fracture surface in the radial zone (zone 2) has an unusual spiral-like character evidently determined by deformation treatment during RF (dynamic deformation of the surface by hard-alloy dies with simultaneous rotation of the sample about its axis).

According to the classification of [25], the fracture surface in the fibrous slow crack growth zone consists of equiaxial dimples, which characterize ductile transgranular fracture; and the fracture surface in the radial zone is determined by a set of dimples directed along a circle, which is determined by the specific feature of RF plastic deformation. According to the classification of [25], the rupture zone of the FG PT-7M alloy sample can be characterized as a set of shear dimples. Note that the fracture of the FG alloy sample, as a whole, has a fairly typical ductile character and, therefore, the noticeable decrease in the ductility of the

PT-7M alloy after RF can be related to the formation of tensile stresses.

The results of HSC tests revealed two types of corrosion defects in the CG PT-7M alloy. The corrosion defects of type I have a characteristic stitch shape (Fig. 7a) related to the stitch arrangement of β-phase particles along α′-phase grain boundaries in the initial alloy structure (Figs. 2a, 2b), and the shape of the corrosion defects of type II is characteristic for the intercrystalline corrosion (ICC) (Fig. 7b). The corrosion layer thickness in the CG PT-7M alloy is 200–300 μm.

The corrosion fracture of the FG PT-7M alloy has another character. For example, after tests for 270 h, pitting corrosion is observed (Fig. 8a); in this case, the corrosion defect depth is no larger than 70 μm. As the test time increases to 320 h, ICC tracks are observed simultaneously with the development of pitting corrosion on the FG alloy surface (Fig. 8b); as the test time increases to 520 h, the ICC defect depth is larger than the fitting corrosion depth by several times (Fig. 8c).

After HSC tests, porous salt precipitates, whose color changes from dark gray to yellow–white, were revealed on the sample surfaces. The formation of pores in salt deposits at the sample surfaces demonstrates the release of gaseous $TiCl_4$ during HSC of the PT-7M titanium alloy [12]. XRD results show that the products of corrosion fracture are a mixture of NaCl and oxide $TiO_2$ in two polymorphic modifications, rutile and anatase.

An analysis of the XRD data demonstrates that, after HSC tests at 250°C for 520 h, $\sigma_{int}$ calculated by the Williamson–Hall method decreases from 440–520 to 110–150 MPa, i.e., to a level close to the internal stresses in the PT-7M alloy in the initial state.

The change in the character of the corrosion fracture of the FG PT-7M alloy with an increase in the test time is thought to be related to the onset of recrystallization, which leads to grain growth. As was shown in [16, 17], intensely migrating grain boundaries in FG α-titanium alloys "sweep out" atoms of corrosion-hazardous alloying elements from the crystal lattice, which leads to an increase in the crystal lattice–grain boundary electrochemical potential difference and, hence, the ICC rate. This assumption corresponds well to the results of studying the structure and properties of the FG PT-7M alloy after HSC tests.

The structure of the FG alloy sample after HSC tests for 270 h has the form characteristic of primary recrystallization: coarse recrystallized grains against the background of a strongly deformed matrix (Figs. 9a, 9b). The average size of coarse grains in the partially recrystallized structure of the sample is ~8.2 μm for the surface layers and ~9.6 μm for the central part of the cross section of the sample. It is evident that the smaller grain size in the surface part of the rod is due to its higher deformation, which leads to an increase in the number of formed recrystallization
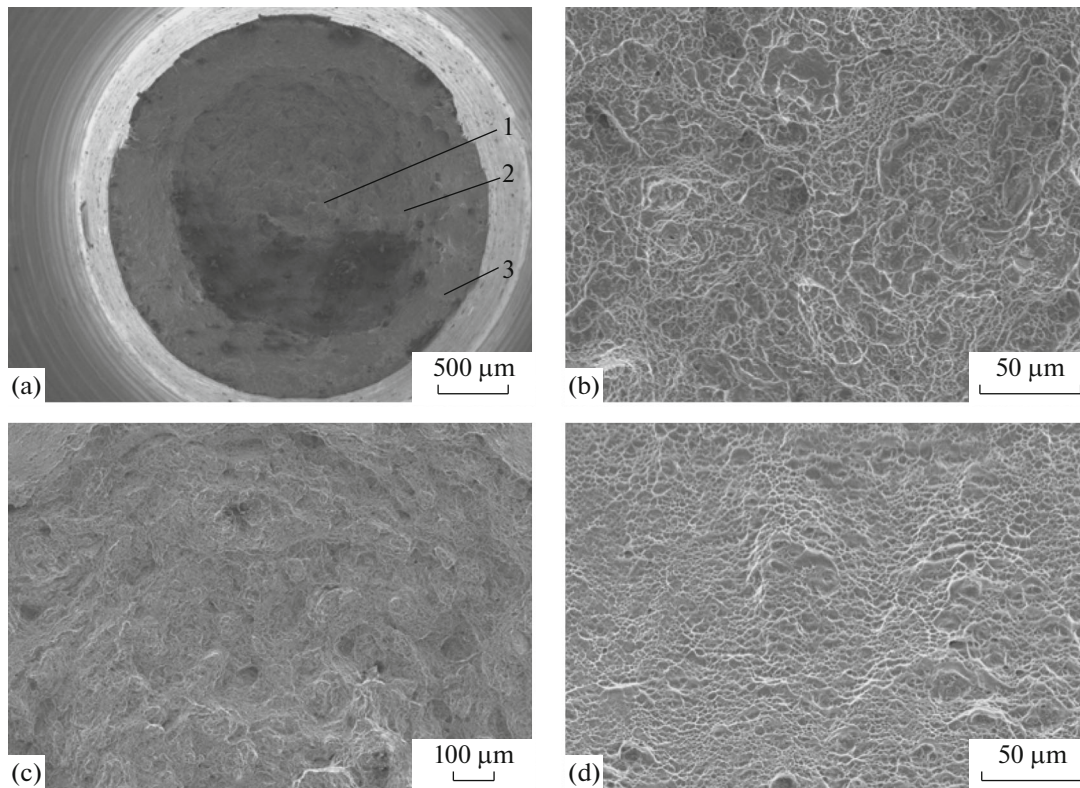
**Fig. 6.** SEM micrographs of the fracture surfaces of the CG PT-7M alloy after tensile tests. (a) General view of fracture: (1) fiber zone of slow crack growth (enlarged image of the zone is shown in (b)), (2) radial zone of fast unstable crack growth (enlarged image of the zone is shown in (c)), and (3) rupture zone (enlarged image of the zone is shown in (d)).
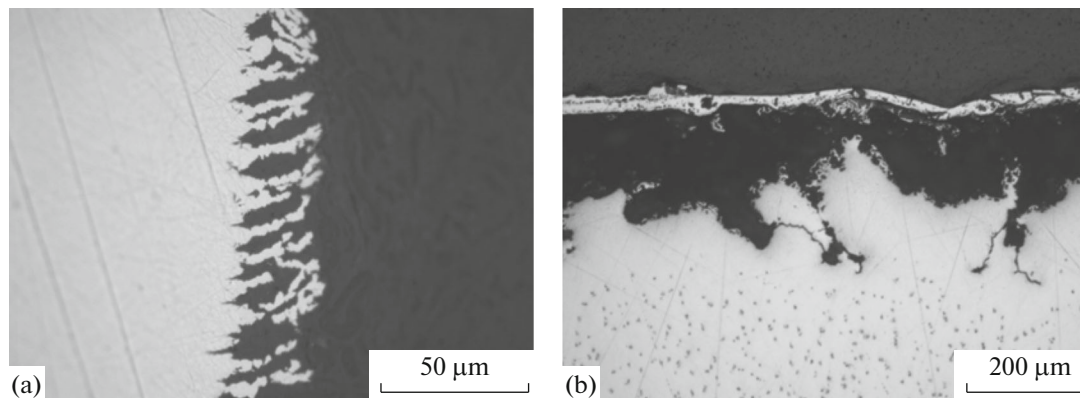


**Fig. 7.** Characteristic shape of corrosion defects on the surface of the CG PT-7M alloy after HSC tests for 520 h: (a) type I (stitch corrosion defects) and (b) type II (ICC).

nuclei, a decrease in the distance between them, and, as a result, a decrease in the average size of recrystallized grains. The microhardnesses of the surface and central parts of the cross section of the PT-7M alloy sample after tests at a temperature of 250°C for 270 h are 2.2 GPa and 2.0−2.1 GPa, respectively, which is noticeably lower than the microhardness of the PT-7M alloy in the state after RF.

The results of studying the structure show that the average grain sizes in the FG PT-7M alloy subjected to HSC tests for 320 and 520 h are 3.5 and 4.2 μm,

respectively. The alloy structure is completely recrystallized after holding for 520 h (Figs. 9c, 9d). The microhardnesses of the samples are 1.8 and 1.7 GPa, respectively. The microhardness in the central part of the cross section of the sample is 100−150 MPa lower than that in the surface layer, and the average grain size in the surface layer is ~0.5−1 μm smaller than that in the central part of the cross section of the sample (Figs. 9c, 9d).

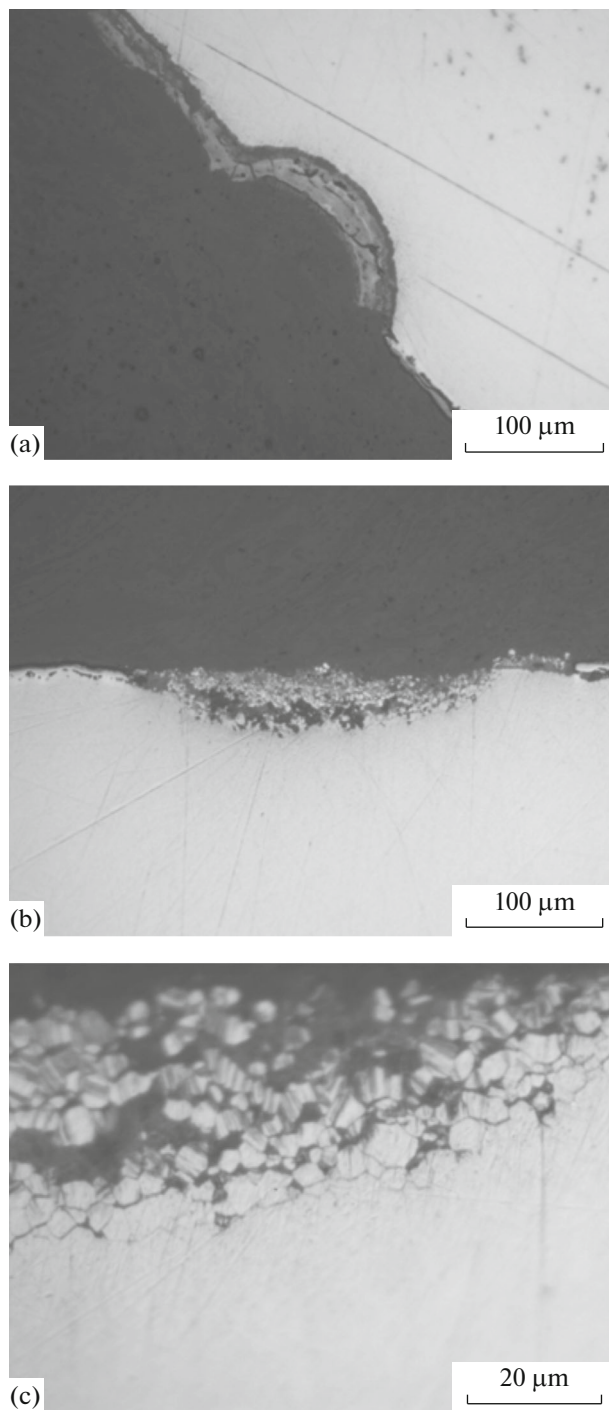An indirect confirmation of the increase in the alloying element concentration on migrating grain

**Fig. 8.** Characteristic shape of corrosion defects on the surface of the FG PT-7M alloy after HSC tests for (a) 270, (b) 320, and (c) 520 h.

boundaries can be the increase in the Hall–Petch coefficient in the recrystallized alloys. As seen in Fig. 10, the slope of the dependence of the microhardness on the average grain size in the $HV_{0.2}-d^{-1/2}$ coordinates is markedly larger in the region of coarse grains than that in the region of small grain sizes. As was

shown in [26−28], the grain-boundary hardening coefficient $K$ in the Hall−Petch equation $HV = HV_0 + Kd^{-1/2}$ characterizes the resistance of grain boundaries to "passage" of lattice dislocations through them, depends substantially on the structural state of grain boundaries, and can increase significantly in the case of formation of grain-boundary segregations (e.g., in pure iron, $K = 0.5$ MPa m$^{1/2}$; in iron alloyed with carbon, $K = 1.6$ MPa m$^{1/2}$ [26]). A similar effect in the ultrafine-grained $\alpha$-titanium alloys fabricated by equal-channel angular pressing was described in [16, 17]. In terms of these concepts, the high value of $K$ in the recrystallized PT-7M alloy after long-term HSC tests can be a result of a high concentration of alloying element atoms on grain boundaries. This fact can lead to a "hardening" of the boundaries, but simultaneously the existence of segregation on grain boundaries sharply decreases the corrosion resistance of titanium alloys [17, 29].

The electrochemical studies of the CG and FG PT-7M alloy samples (Fig. 11) show that, during FG structure formation, corrosion current density $j_{cor}$ for the metal of the central part of the longitudinal section of the sample is 1.14−1.16 mA/cm$^2$ (Fig. 1, zone 1). In this case, corrosion potential $E_{cor}$ of the material of the sample central part (zone 1) is −(482−492) mV. The corrosion current density at the sample surface (zone 2) of the FG PT-7M alloy after RF is $j_{cor} = 0.80-$ 0.94 mA/cm$^2$ ($E_{cor} = -(483-492)$ mV. Thus, the strongly deformed surface layer of the FG PT-7M alloy sample (zone 2) with a high hardness ($HV_{0.2} = $ 2.9−3.0 GPa) has higher corrosion resistance (lower corrosion current density $j_{cor}$ and corrosion potential $E_{cor}$) as compared to the central part of the sample (zone 1) with a lower hardness ($HV_{0.2} = 2.5-2.6$ GPa). For the CG PT-7M alloy with a hardness of 1.9− 2.0 GPa, the mean corrosion current density is $j_{cor} = $ 1.07 mA/cm$^2$ ($E_{cor} = -465$ mV), although the properties of the initial rod exhibited a noticeable scatter from sample to sample. Generalized data on the obtained results are given in Table 1.

Note that the higher corrosion resistance of the surface layer of the rod is a quite unexpected result, since it is traditionally assumed that an increase in the strain of a metal should lead to an increase in the rate of its corrosion failure [30−33].

An analysis of the results of metallographic studies of the sample surface after electrochemical tests demonstrates that the corrosion process during the tests of the CG alloy occurs mainly due to etching of interphase ($\alpha-\beta$) boundaries (Figs. 12a, 12b). The character of the corrosion fracture of the FG sample surface is different and characterized by etching of localized deformation bands (Figs. 12c, 12d).

This effect is thought to be explained by the fact that the localized deformation bands in the surface layer of the titanium rod are arranged much closely to
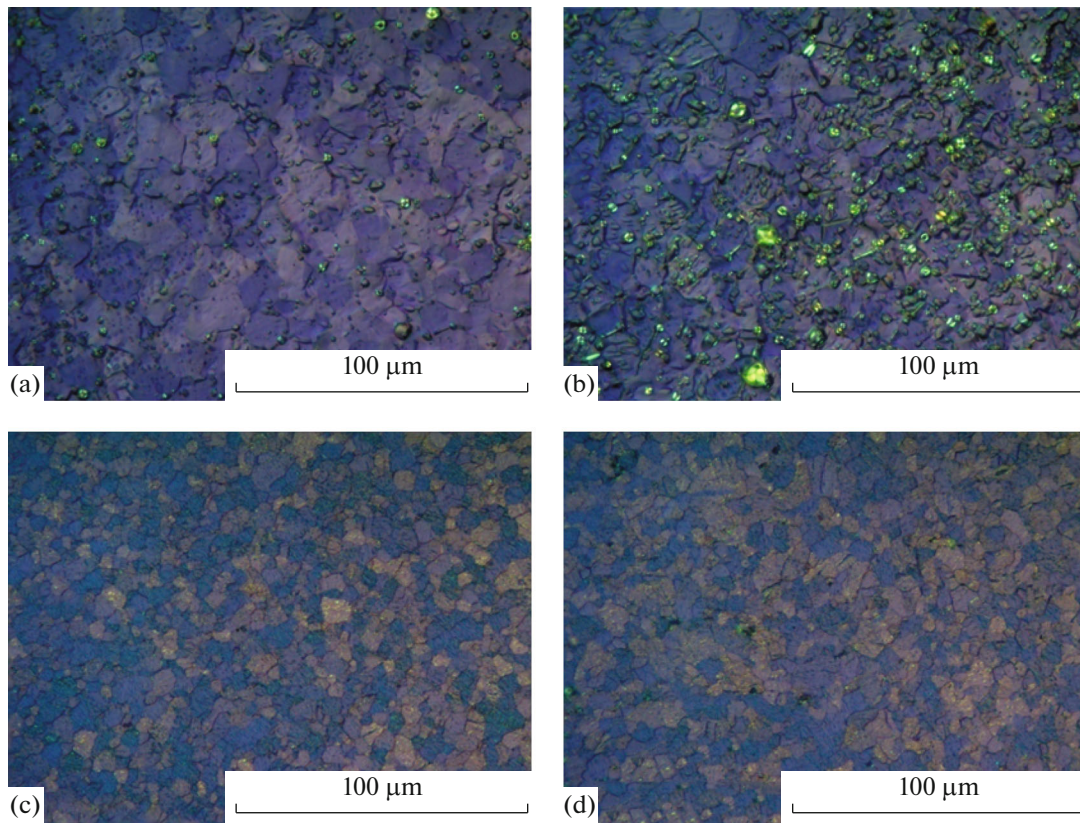
**Fig. 9.** Microstructures of (a, c) edge and (b, d) central parts of the cross section of the FG PT-7M alloy after HSC tests for (a, b) 270 and (c, d) 520 h. Interference contrast.
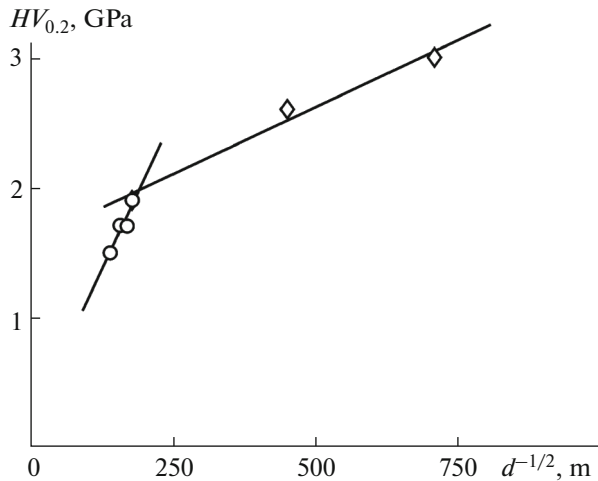


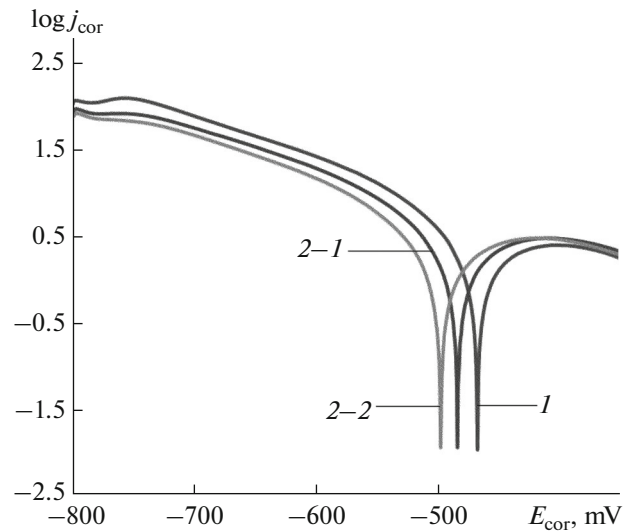**Fig. 10.** Microhardness $HV_{0.2}$ vs. grain size $d$ for the FG PT-7M alloy after HSC tests.



**Fig. 11.** Results of electrochemical studies ($j_{cor}$ is the corrosion current density, mA/cm$^2$) of (*1*) CG and (*2*) FG PT-7M alloys (*2-1* and *2-2* are the central part of the cross section and the surface layer of the FG sample, respectively).

each other as compared to the central part, and they almost overlap near the surface.[3] This finding can lead to the absence of alternating parts of strongly and weakly deformed structures in the metal with different

electrochemical properties, which are peculiar analogs of "microgalvanic pairs" (which provoke accelerated dissolution of the metal). In addition, a change in the electrochemical corrosion conditions at the α-phase/β-

---

[3] The high corrosion resistance of surface layers of titanium rods with a high degree of a preliminary deformation as compared to the metal in the central zone of the cross section of the rod.

**Table 1.** Results of electrochemical studies of titanium PT-7M alloy samples after RF

| State of material | Region of study (see Fig. 1) | $HV_{0.2}$, MPa | $j_{cor}$, mA/cm$^2$ | $E_{cor}$, mV |
|---|---|---|---|---|
| After RF | Center of rod (zone 1) | 2.5–2.6 | 1.14–1.16 | −(482–485) |
| | Rod surface (zone 2) | 2.9–3.0 | 0.80–0.94 | −(483–492) |
| Initial CG state | | 1.9–2.0 | 1.07 | −465 |

phase interface can favor an increase in the corrosion resistance of the deformed parts of the titanium alloy. The β phase of titanium is known to have a more negative electrode potential ($E_β$) than that of the α phase ($E_α$), which, in particular, leads to intense etching of the interface during corrosion tests (Figs. 2b, 11a, 11b) and a shift of corrosion potential $E_{cor}$ in two-phase (α + β) alloys (VT6, VT16, etc.) to the region of more negative corrosion potentials as compared to pure titanium [34].

The plastic deformation of grains leads to an increase in the lattice dislocation density and decreases the electrode potential of the α-phase (i.e., shifts potential $E_α$ to the region of more negative val-

ues) [34, 35]. This fact implies that the difference in the corrosion potentials of the α and β phases ($ΔE = E_α − E_β$) would decrease and, hence, weaken the contribution of α/β interphase boundaries to the intensity of the corrosion failure of the FG titanium alloy. An additional factor, which also favors a decrease in the contribution of α/β interphase boundaries, is the refinement of β-phase particles during plastic deformation.

These results demonstrate increased corrosion resistance of the FG PT-7M alloy as compared to the initial state and also a change in the corrosion (electrochemical) failure mechanism of the PT-7M alloy
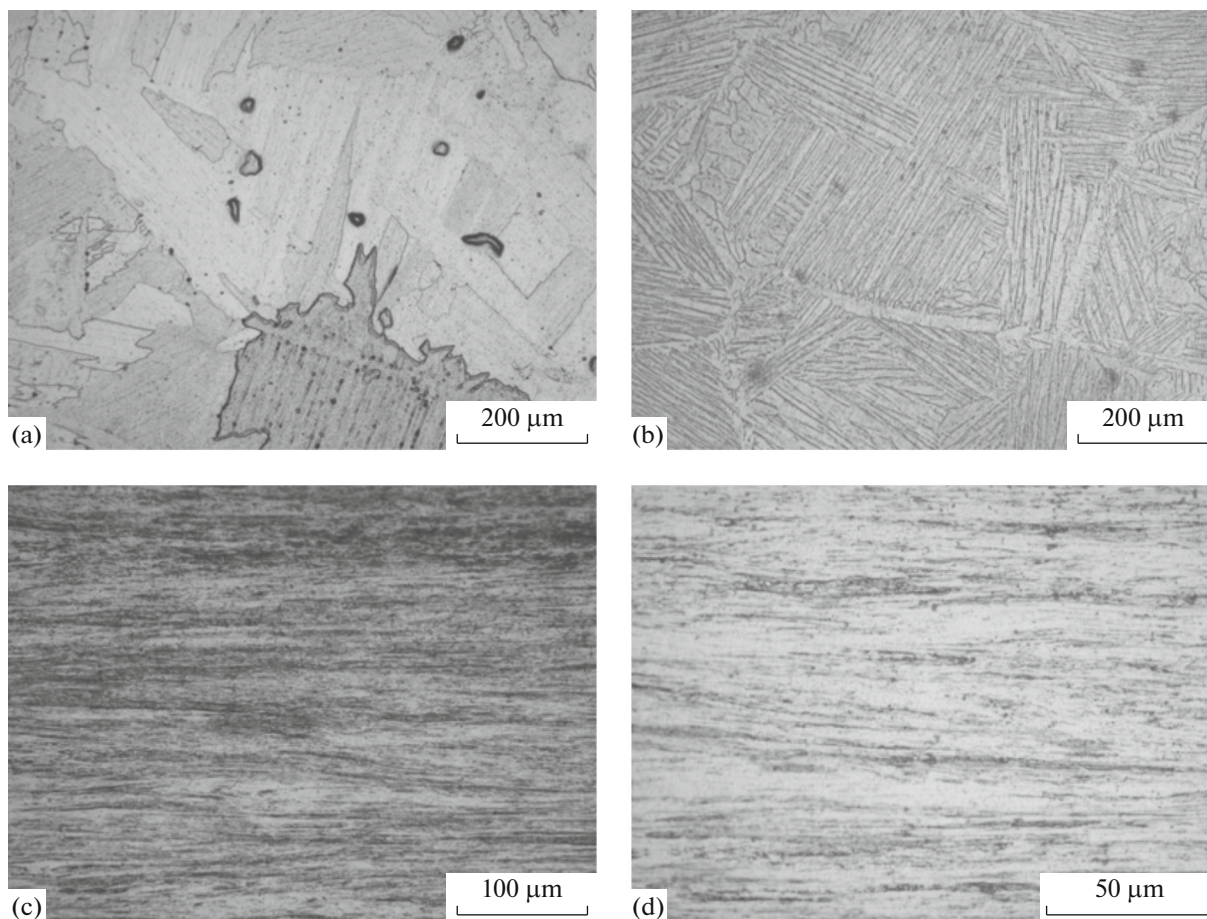


**Fig. 12.** Surface structure of (a, b) CG and (c, d) FG PT-7M alloys after electrochemical tests: (c) surface layer of the FG alloy and (d) central layer of the FG alloy.

during the formation of a grain/subgrain FG structure in it.

## CONCLUSIONS

(1) RF of an α-titanium PT-7M alloy is found to lead to the formation an FG structure with high mechanical properties: the yield strength is $\sigma_{0.2} = 1050-1070$ MPa, the ultimate tensile strength is $\sigma_u = 1080$ MPa, and the microhardness is $HV_{0.2} = 2.9-3.0$ GPa. After RF, tensile internal stress fields making an additional contribution to a decrease in the ductility alloy form in the alloy: the relative elongation to failure is $\delta_5 = 6-8\%$.

(2) HSC tests for 520 h demonstrate the formation of two types of corrosion defects at different depths at the surface of the CG α-titanium PT-7M alloy. They related to the stitch precipitation of β-phase microparticles along grain boundaries of the $\alpha(\alpha')$ phase (defects of type I) and intercrystalline corrosion (defects of type II). The existence of the type-II defects is due to an increased concentration of corrosion-active alloying elements (zirconium, aluminum) at grain boundaries of in CG PT-7M alloy.

(3) The fracture of the FG alloy during HSC was found to be dependent on the test time and to change from pitting corrosion to intercrystalline fracture when the test time increases from 270 to 500 h. The change in the corrosion fracture of the FG alloy is due to the onset of recrystallization, during which intensely migrating grain boundaries sweep out the corrosion-active alloying elements distributed in the lattice volume of the titanium alloy.

(4) The formation of an FG structure was found to increase the electrochemical corrosion resistance of the titanium alloy. The corrosion resistances of the surface and the central zones of the cross section of the PT-7M alloy samples are different, which is likely to be due to the differences in the strain accumulated in the central and surface layers of the rod during RF. The corrosion failure of the surface of the CG alloy during electrochemical tests was shown to occur via etching of α/β interphase boundaries. Active corrosion etching of localized deformation bands was observed in FG PT-7M alloy.

## FUNDING

## REFERENCES

1. I. V. Gorynin, S. S. Ushkov, A. N. Khatuntsev, and N. I. Loshakova, *Titanium Alloys for Marine Engineering* (Politekhnika, St. Petersburg, 2007).

2. A. S. Gornakova, V. V. Straumal, and S. I. Prokofiev, "Coarsening of (αTi) + (βTi) microstructure in the Ti–Al–V alloy at constant temperature," Advanc. Eng. Mater. Paper code 1800510 (2018).

3. S. V. Zherebtsov, E. A. Kudryavtsev, G. A. Salishchev, B. B. Straumal, and S. L. Sematin," Microstructure evolution and mechanical behavior of ultrafine Ti–6Al–4V during low-temperature superplastic deformation," Acta Mater. **121**, 152–163 (2016).

4. V. I. Betekhtin, Yu. R. Kolobov, V. Sclenichka, A. G. Kadomtsev, M. V. Narykova, J. Dvorak, E. V. Golosov, B. K. Kardashev, and I. N. Kuz'menko, "Effect of a defect structure on the static and long-term strength insubmicrocrystalline VT1-0 titanium fabricated by plastic deformation during screw and lengthwise rolling," Tech. Phys. **60** (1), 66–71 (2015).

5. S. V. Zherebtsov, "Efficiency of the strengthening of titanium and titanium alloys of various classes by the formation of an ultrafine-grained structure via severe plastic deformation," Russ. Met. (Metally) No. 11, 969–974 (2012).

6. S. V. Rogozhkin, A. A. Nikitin, N. N. Orlov, T. V. Kulevoi, P. A. Fedin, O. A. Korchuganova, M. A. Kozodaev, A. L. Vasil'ev, A. S. Orekhov, N. N. Kolobylina, V. P. Leonov, and I. A. Schastlivaya, "Microstructure of Ti–5Al–4V–2Zr titanium alloy in the initial state and after irradiation by titanium ions," Perspect. Mater., No. 12, 5–15 (2016).

7. V. I. Betekhtin, O. R. Kolobov, M. V. Narykova, B. K. Kardashev, E. V. Golosov, and A. G. Kadomtsev, "Mechanical properties, density, and defect structure of VT1-0 titanium after intense plastic deformation due to screw and longitudinal rolling," Tech. Phys. **56** (11) 1599–1604 (2011).

8. V. P. Leonov, E. V. Chudakov, and Yu. Yu. Malinkina, "Effect of ruthenium microadditions on the structure, corrosion–mechanical strength and the fractography of fracture of pseudo-α-titanium alloys," Materialovedenie, No. 1, 3–11 (2017).

9. G. A. Salishchev, R. M. Galeev, S. P. Malysheva, S. V. Zherebtsov, S. Yu. Mironov, O. P. Valiakhmetov, and E. F. Ivasenko, "Formation of subnicrocrystalline structure in titanium and titanium alloys and their mechanical properties," Materialoved. Term. Obrab. Met., No. 2 (608), 19–26 (2006).

10. I. V. Ratochka, O. N. Lykova, and E. V. Naidenkin, "Influence of low-temperature annealing time on the evolution of the structure and mechanical properties of a titanium Ti–Al–V alloy in the submicrocrystalline state," Phys. Met. Metallograph. **116** (3), 302–308 (2015).

11. D. Sinigaglia, G. Taccani, and B. Vicentini, "Hot-salt-stress-corrosion cracking of titanium alloys," Corros. Sci. **18**, 781–796 (1998).

12. Thierry Chevrot, "Pressure effects on the hot-salt stress-corrosion cracking of titanium alloys," PhD Thesis, Cranfield University, 1994.

13. V. V. Zakharova, "Influence of air oxygen and the salt precipitate thickness on the corrosion cracking of titanium alloys at high temperatures in contact with NaCl," Trudy VIAM, No. 10, 12 (2014).

14. V. V. Zakharova, "Influence of the chemical composition, heat treatment, and structure on the resistance of

titanium alloys to cracking due to hot salt corrosion," Trudy VIAM, No. 9(45), 11 (2016).

15. V. N. Chuvil'deev, V. I. Kopylov, A. V. Nokhrin, A. M. Bakhmet'ev, N. G. Sandler, P. V. Tryaev, N. A. Kozlova, N. Yu. Tabachkova, A. S. Mikhailov, M. K. Chegurov, and E. S. Smirnova, "Effect of the local chemical composition of grain boundaries on the corrosion resistance of a titanium alloy," Tech. Phys. Let. **43** (1), 5—8 (2017).

16. V. N. Chuvil'deev, V. I. Kopylov, A. V. Nokhrin, A. M. Bakhmet'ev, N. G. Sandler, N. A. Kozlova, P. V. Tryaev, N. Yu. Tabachkova, A. S. Mikhailov, A. V. Ershova, M. Yu. Gryaznov, M. K. Chegurov, A. N. Sysoev, and E. S. Smirnova, "Simultaneous increase in the strength, plasticity, and corrosion resistance of an ultrafine-grained Ti—4Al—2V pseudo-α-titanium alloy," Tech. Phys. Let. **43** (5), 466—469 (2017).

17. V. N. Chuvil'deev, V. I. Kopylov, A. V. Nokhrin, P. V. Tryaev, N. A. Kozlova, N. Yu. Tabachkova, Yu. G. Lopatin, A. V. Ershova, A. S. Mikhailov, M. Yu. Gryaznov, and M. K. Chegurov, "Study of mechanical properties and corrosive resistance of an ultrafine-grained α-titanium alloy Ti—5Al—2V," J. Alloys Comp. **723**, 354—367 (2017).

18. V. M. Segal, I. J. Beyerlein, C. N. Tome, V. N. Chuvil'deev, and V. I. Kopylov, *Fundamentals and Engineering of Severe Plastic Deformation* (Nova Sci. Publ., New York, 2010). ISNB 978-1-61668-190-6.

19. V. Segal, "Review: modes and processes of severe plastic deformation," Materials **11** (7), 1175 (2018).

20. O. K. Dedyulina, G. A. Salishchev, and A. S. Pertsev," Materialoved. Term. Obrab. Met., No. 3 (729), 7—12 (2016).

21. V. N. Serebryanyi, I. A. Malyshev, D. N. Tsaikler, N. S. Martynenko, M. M. Morozov, and S. V. Dobatkin, "Texture and deformation mechanisms in MA2-1pch magnesium alloy during rotary forging," Zav. Labor. **84** (8), 25—31 (2018).

22. S. V. Zherebtsov, M. A. Boeva, G. A. Salishchev, E. A. Kudryavtsev, A. S. Pertsev, V. V. Latysh, I. V. Kandarov, "Effect of warm rotary forging on the structure and properties of VT6 titanium alloy," Vestn. Ufa State Aviats. Eng. Univer. **16** (7 (52)), 30—34 (2012).

23. G. K. Williamson and W. M. Hall, "X-ray line broadening from field aluminium and wolfram," Acta Metal. **1** (1), 22—31 (1953).

24. E. A. Borisova, G. A. Bochvar, M. Ya. Brun, et al., *Metallography of Titanium Alloys*. Ed. by N. F. Antoshkin (Metallurgiya, Moscow, 1980).

25. A. Ferrows, *Fractography and Atlas of Fractographs in Metals Handbook* (Metals Park, Ohio, 1974), Vol. 9.

26. I. E. Dolzhenkov and I. I. Dolzhenkov, *Spheroidization of Carbides in Steel* (Metallurgiya, Moscow, 1984).

27. V. N. Chuvil'deev, A. V. Nokhrin, M. M. Myshlyaev, V. I. Kopylov, Yu. G. Lopatin, N. V. Melekhin, A. V. Piskunov, A. A. Bobrov, and O. E. Pirozhnikova, "Effect of recovery and recrystallization on the Hall—Petch relation parameters in submicrocrystalline metals: I. Experimental studies," Russ. Met. (Metally) No. 1, 71—89 (2018).

28. V. N. Chuvil'deev, A. V. Nokhrin, M. M. Myshlyaev, V. I. Kopylov, Yu. G. Lopatin, N. V. Melekhin, A. V. Piskunov, A. A. Bobrov, and O. E. Pirozhnikova, "Effect of recovery and recrystallization on the Hall—Petch relation parameters in submicrocrystalline metals: II. Model for calculating the Hall—Petch relation parameters," Russ. Met. (Metally) No. 5, 487—499 (2018).

29. B. B. Cheulin, S. S. Ushkov, I. N. Razuvaeva, and V. N. Goldfain, *Titanium Alloys in Mechanical Engineering* (Mashinostroenie, Leningrad, 1977).

30. N. D. Tomashov and G. P. Chernova, *Theory of Corrosion and Corrosion-Resistant Structural Alloys* (Metallurgiya, Moscow, 1986).

31. F. N. Tavadze and S. N. Mandzhgaladze, *Corrosion Resistance of Titanium Alloys* (Metallurgiya, Moscow, 1969).

32. N. D. Tomashov and R. M. Al'tovskii, *Corrosion and Titanium Protection* (Mashgiz, Moscow, 1963).

33. N. D. Tomashov, *Titanium and Corrosion-Resistant Titanium-Based Alloys* (Metallurgiya, Moscow, 1985).

34. N. A. Amirkhanova, R. Z. Valiev, E. Yu. Chernyaeva, E. B. Yakushina, and I. P. Semenova, "Corrosion behavior of titanium materials with an ultrafine-grained structure," Russ. Met. (Metally), No. 5, 456—460 (2010).

35. V. V. Gerasimov, *Prediction of Metal Corrosion* (Metallurgiya, Moscow, 1989). ISBN 5-229-00513-0.

*Translated by Yu. Ryzhkov*